We are IntechOpen,
the world's leading publisher of
Open Access books
Built by scientists, for scientists

4,800
Open access books available

122,000
International authors and editors

135M
Downloads

Our authors are among the

154
Countries delivered to

TOP 1%
most cited scientists

12.2%
Contributors from top 500 universities

CLARIVATE ANALYTICS
BOOK CITATION INDEX
INDEXED

WEB OF SCIENCE™

Selection of our books indexed in the Book Citation Index
in Web of Science™ Core Collection (BKCI)

Interested in publishing with us?
Contact book.department@intechopen.com

Numbers displayed above are based on latest data collected.
For more information visit www.intechopen.com

Building Partial Discharge Signal Wireless Probes

Fabio Viola and Pietro Romano

Additional information is available at the end of the chapter

1. Introduction

In the recent years compact ultra-wideband (UWB) antennas have received a great attention [1-3] due to the allocation of various frequency bands to UWB systems by Federal Communications Committee (FCC) [4]. One of the most interesting aspects of these antennas is their aptitude of detecting electromagnetic (EM) transients with frequency content up to the very high frequency (VHF) range. EM transient phenomena with the above mentioned frequency content are those encountered, for example, in partial discharge (PD) detection. This diagnostic method is now widely used to identify defects taking place in the insulation systems. Wireless systems offer the possibility to achieve the whole shape of PD signals radiated from the source of the PD defects with less distortion due to the electric transmission path.

Modern diagnostic procedures require clear PD patterns for the identification of defects generating PD because different defects can affect differently the insulation reliability, [5-7]. Different pulsating sources can be simultaneously active during a PD measurement session and mixed PD patterns can be recorded. Thus, an effective separation of mixed PD patterns into sub-patterns each one pertinent to a specific noise or PD source typology, is a fundamental task to avoid wrong defect identification, [8-9]. One of the possible approaches in signal separation is based on the assumption that the same defect generates similar waveforms and features derived from signals grouped by similarity can be adopted to identify the defect or noise source. Thus, the dynamic characteristics of the antenna probe must be designed/ evaluated in order to fit the above mentioned requirements.

Both the time and the frequency domain can be used for separation purposes. Recently, the use of the Auto-Correlation Function (ACF) has been proposed for its ability to synthesize both the time and frequency domain features as well as to be less affected by superimposed high-frequency noise, random truncation of the pulse-tail (frequency leakage) and different trigger activation, [10].

INTECH
open science | open minds

The ACF has been adopted here to evaluate the performances of different EM probes in order to design the more suitable geometry to build a portable low-cost device for PD detection. Monopole, triangular and spherical antennas were simulated by means of the surface Method of Moments (MoM) in the frequency domain, [11-14]. The transmitting system is modeled by a power electronic device with a fault current between two metal plates. The ACF shapes of the simulated, transmitted and received signals, have been compared using the Pearson correlation index to verify which sensor is providing the best fidelity among the three.

This chapter focuses on the evaluation of the performances of different antenna sensors suitable for Partial Discharge (PD) measurements. Monopole, triangular and spherical antennas were simulated by means of the surface method of moments. The transmitting system is modeled by a power electronic device with a fault current between two metal plates. The shape of the simulated, transmitted and received signals, has been compared to verify the sensor that provides the best fidelity among the three. The auto-correlation function and the Pearson correlation index are adopted here for the comparison. A discussion on the dynamic characteristic of the different antenna probes and their use in different application is proposed.

2. Partial discharges

The increasing necessity of high voltage levels in high voltage (HV) power systems has driven to a stronger demand of insulating materials with high electrical performances at affordable costs. Since synthetic polymers partially meet these requirements [15, 16], they have been studied quite a bit in the most recent literature. However, they are affected by some aging problems also the PD phenomenon is a major cause of failure in the insulation systems of electrical apparatus. These discharges take place in consequence of unavoidable local defects produced by the industrial manufacturing process, and promote local erosion of the material that may cause electric breakdown of the component over time. The difficulty of performing reliable life predictions and suitable evaluations of their reliability in presence of such degradation phenomena, hindered a wide diffusion of HV components made of epoxy materials. The diagnostic techniques of recognition, identification and classification of discharge phenomena are therefore fundamental for the evaluation of the time reliability of the electrical equipment, especially for high voltages. In order to study and understand the behaviour of different materials, the first step is to perfectly know the dielectric characteristics. Materials are divided into three basic categories that are metals, ceramics and polymers. Furthermore, the combination of two or more of these elements gives rise to materials employed in common applications normally named composite materials. Successively, another division is based on the type of atomic bond and on the basis of the crystal structure that composes them. Besides, in solid state physics, the electronic band structure of a solid describes the range of energies that an electron of a certain material is "allowed" or "forbidden" to possess. The electronic structure of a material greatly is influencing the materials behaviour and the energy gap between the valence band. The conduction is used to classify the materials on the electronic characteristics, in conductors, semiconductors and insulators. The insulators materials or dielectric materials present a wide forbidden zone between the valence band and

the conduction band. Dielectric materials are divided into three categories named solid, liquid and gaseous. The main electrical properties that characterize the behaviour of insulating materials are:

- *Intrinsic/extrinsic conductivity*σ and γ are about $10^{-5} \div 10^{-18}$ [S/m].

- *Electric permittivity* $\varepsilon_r = \varepsilon/\varepsilon_0$; where ε is the permittivity of a generic material and ε_0 is the vacuum dielectric permittivity with value $8 \bullet 85418781762 \times 10^{-12}$ [F/m].

- *Loss factor*, defined as tgδ with $\delta = 90° - \varphi$, the loss angle of the material, with φ the phase shift between voltage and current, which, in the ideal case is equal to 90° while, in a real dielectric, is less than 90° due to their leaks.

- *Dielectric Rigidity* (RD):value of the voltage gradient required to cause discharge through the dielectric under examination or the limit value of the electric field beyond which produces a conduction of electricity (electrical discharge) through the dielectric material. It is commonly measured in kV/mm. The discharge gradient is strongly influenced bya very high number of different parameters and by the test procedure, in particular by the shape of electrodes, by the voltage applied and by the way the limit voltage is reached.

The Test procedures for these characteristic parameters depending on the dielectric materials state are often very different. To better understand the partial discharge phenomenon, the discharge base theory in gas is synthetically presented in the next section, while extended information are reported in [15, 16]. Gaseous insulation, especially ambient air, is the most commonly used insulation in high voltage engineering.

2.1. Discharge theory

The occurrence of partial discharges in electrical equipment has been identified as one of the main causes of breaking devices and reduction in useful life of insulation. For many years, studies on the physical and chemical aspects of PD have been thoroughly addressed and news discharge models were introduced. The principle of discharge starting mechanism, for small distances, was introduced by Towsend [15, 16] and it is based on the coefficient of ionization of the gas subjected to an electric field. For distances more than a few millimetres, Towsend theory is wrong, since discharge develops in a times lower than necessary ones for electrons to cross the distance between electrodes and form an avalanche. To explain the formation of the discharge's mechanism over long distances, several assumptions were made based on phenomenon such as the formation of individual electronic avalanches or photo-ionization phenomena. Meek and Loeb, and independently Rather, proposed the Streamer theory. The equations that describe phenomena involving electrons and ions, avalanches and streamers, are too complex to be dealt with in a few lines and can be found in [15,16].

It is possible to macroscopically represent the discharge phenomenon with a circuit model. This one is representing the system cavity-electrodes in the dielectric. The Whitehead model is exhibiting three capacitors to represent a cavity embedded in a dielectric. Fig. 1 details this model [17].
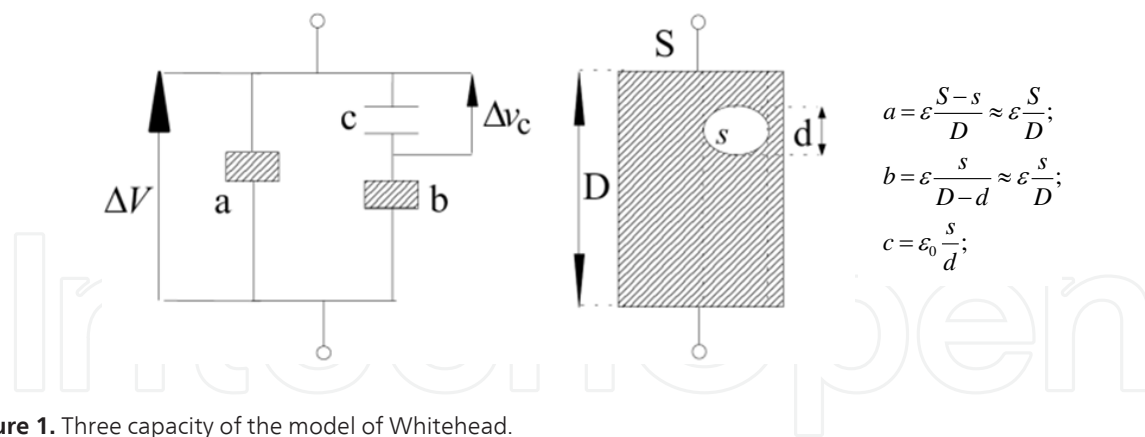
Figure 1. Three capacity of the model of Whitehead.

Fig. 2 presents the V_c voltage applying on the c capacitor. It should be noticed that V_c is a fraction of the total voltage V. When V_c exceeds the so called inception voltage V_{ci}, the discharge starts. After the discharge, V_c reaches the discharge extinction voltage value, V_{ce}. The global behaviour of the system is affected and the PD activity can be monitored by employing current and voltage measures.
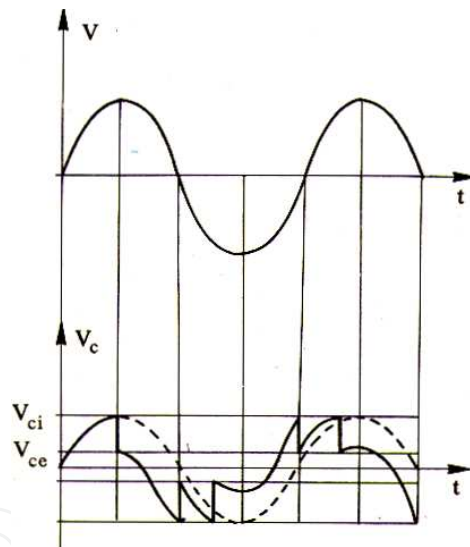

Figure 2. V voltage applied to the dielectric, V_c voltage across the cavity, V_{ci} inception voltage of the discharge, V_{ce} discharge extinction voltage.

A field approach model that best represents the phenomenon is conceived by Pedersen [18]. Since the charge involved by the discharge inside the cavity, named true charge, cannot be measured, an auxiliary current, named apparent charge, is measured outside of the specimen. The phenomenon is then traced to two successive stages:

- the first defines the external current measured with the induced charge to the electrodes.

- the second one correlates the induced charge to the electrodes with the charge inside the cavity.

2.2. Partial discharge characterization

A partial discharge is a stochastic phenomenon that involves many chemical and physical aspects of materials proprieties. The PD detection over time has become an indispensable method for the evaluation of insulation systems in the realization phase of new devices but also for evaluate reliability in work. The discharge manifests itself through charge displacement, acoustic waves, lights and electromagnetic field. The wired detection of charge displacement was the most frequently measurement method chosen before the introduction of antenna probes. The basic discharge detection circuit, in accordance with the International Electrotechnical Commission (IEC) Standard, is shown in fig. 3 [19]. The coupling capacitor provides a low impedance path for high-frequency discharge currents which cause voltage pulses over the measuring impedance. The pulses are then amplified and stored in a computer for further processing and displayed in different patterns as 3D patterns (phase-amplitude-number of discharge) and 2D patterns (amplitude-number, phase-number, phase-amplitude).

In the same IEC Standard the main definitions related to PD are defined as follows:

Partial discharge (PD): Localized electrical discharge that only partially bridges the insulation between conductors and which can or cannot occur adjacent to a conductor.

Partial discharge pulse (PD pulse): Current or voltage pulse that results from a partial discharge occurring within the object under test. The pulse is measured using suitable detector circuits, which have been introduced into the test circuit for the purpose of the test.

Apparent charge q: Of a PD pulse is that charge which, if injected within a very short time between the terminals of the test object in a specified test circuit, would give the same reading on the measuring instrument ad the PD current pulse itself. The apparent charge is usually expressed in picocoulombs (pC).

Pulse repetition rate n: Ratio between the total number of PD Pulses recorded in a selected time interval and the duration of this time interval.

Phase angle ϕ_i and time t_i of occurrence of a PD pulse: is $\phi_i=360(t_i/T)$ where t_i is the time measured between the preceding positive going transition of the test voltage through zero and the partial discharge pulse and T is the period of the test *voltage.*

The pulses generated by PDs are detected as second order pulses; in Fig.4 the pulse was recorded by means of an oscilloscope and shows a signal proportional to the discharge current. It was detected by means of a 50 Ω resistance in series to the circuit where the defect was present. This kind of pulses are very fast (~50ns) and have a small amplitude (~5mV). As we will see in the following, not only the amplitude of the pulse but also its duration is a fundamental parameter. The most important recent studies that have allowed PD measurements to become a reliable diagnostic system are based on the shape of the pulses, and in particular on the ratio between duration and frequency content. The acquisition techniques (bandwidth of the recording system) and the kind of sensor adopted (HFCT, capacitive couplers) become fundamental components because they affect the shape of the impulses.
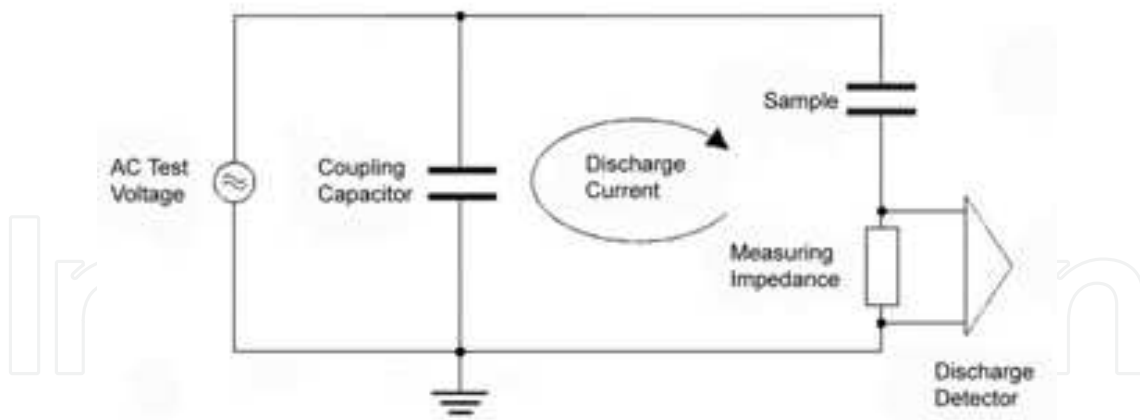
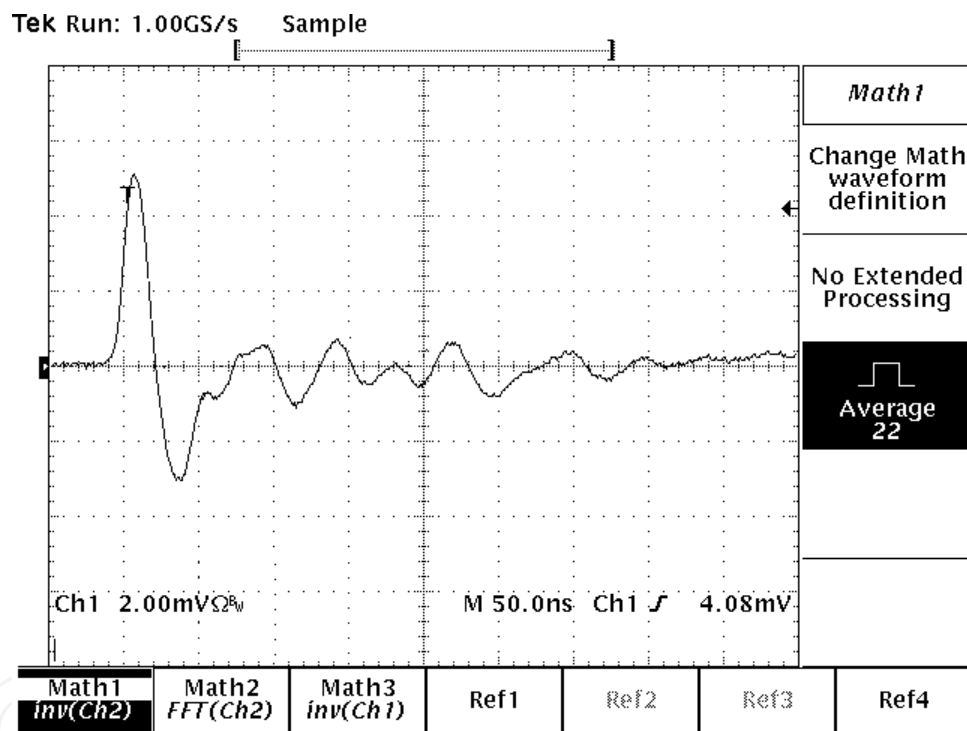**Figure 3.** Discharge detection circuit.

Figure 4. Generic second order PD Pulse.

In the PD detection theory, three families of PD phenomena have been taken into account: namely internal, surface and corona. Internal discharges occur inside a cavity embedded in a dielectric. These are cavities within resin components, extruded plastic cables, joint, stator insulation and external particles such as dust or textile fibres embedded in insulation. Surface discharge may occur along dielectric surfaces with a high tangential field stress. Typical examples of high voltage components that present surface discharges are bushing, twisted pairs, ends of cables, the overhang of generator windings. Corona discharges occur in a needle plane configuration at sharp points at high voltage or ground potential [20].

The pulse shape of singular discharge phenomena present differences in term of time duration and frequency content. These differences are exhibited in Fig. 5 where an example of pulse shape and frequency spectrum for each discharge family is showed.
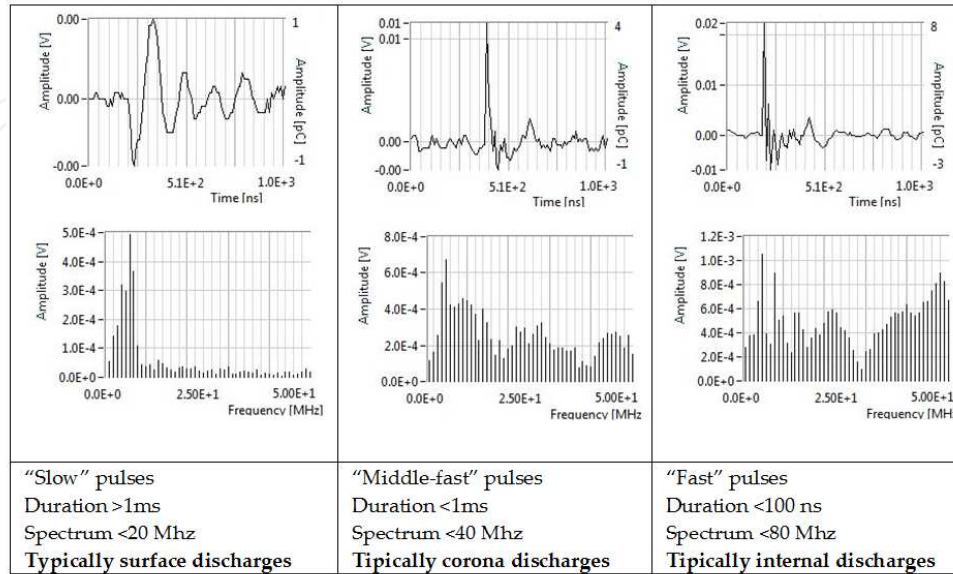

"Slow" pulses	"Middle-fast" pulses	"Fast" pulses
Duration >1ms	Duration <1ms	Duration <100 ns
Spectrum <20 Mhz	Spectrum <40 Mhz	Spectrum <80 Mhz
Typically surface discharges	**Tipically corona discharges**	**Tipically internal discharges**

Figure 5. Time duration and frequency spectrum of surface, corona and internal discharges.

Moreover, the acquisition of the pulse repetition on a time interval ΔT is displayed in a 3D histogram generally known as PD Pattern (phase-amplitude-number of discharge) and 2D PD patterns (amplitude-number, phase-number, phase-amplitude,) as displayed in Fig.6. Furthermore, the pattern allows the understanding of the kind of the defect.We obtain different patterns for each discharge family as shown in Fig.7, 8 and 9.
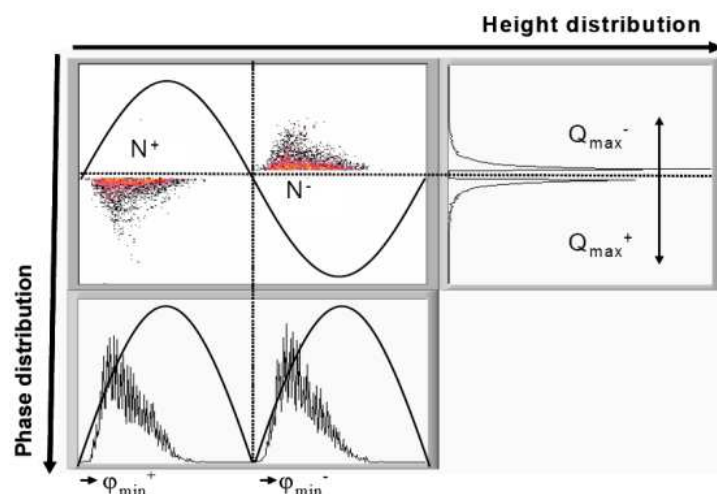

Figure 6. PD Pattern with 2D amplitude-number (right) and phase-number (below). In the 3D PD Pattern the colour scale represents the intensity of the discharges.

Fig.7 shows a typical internal void rabbit-like PD pattern. Internal discharge are characterized by a quite symmetry for positive and negative discharges due to electron emission from the same materials (dielectric). In particular the showed pattern is referred to a spherical air void embedded in a dielectric subjected to a uniform electric field.
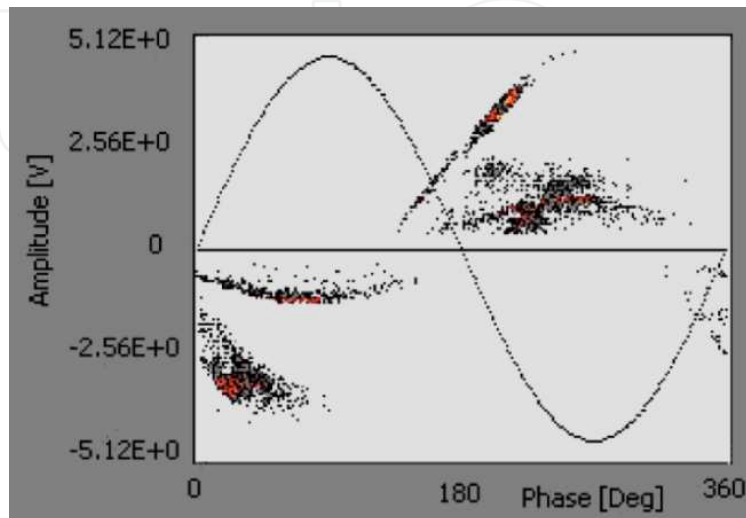

Figure 7. PD Pattern of internal discharges.

Fig.8 shows a typical surface PD pattern, where a substantial dissymmetry between positive and negative discharges can be noted. The inception phase angle, $\Delta\phi$, defined as the phase interval between the first and the last discharge (positive or negative) is smaller than the one observed for internal discharges.
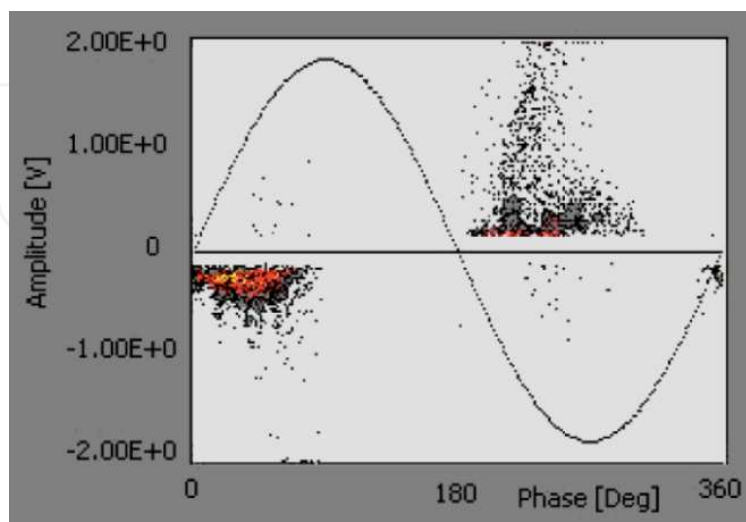

Figure 8. PD Pattern of surface discharges.

Fig.9 shows a typical corona PD pattern. Two characteristic differentiates it from the previous discharges. The first is the presence of discharge only in half period of AC source and the second is that the discharge occurs in correspondence of the voltage pick of AC source, in the other cases, differently, the discharges occur in presence of the maximum gradient of the voltage.
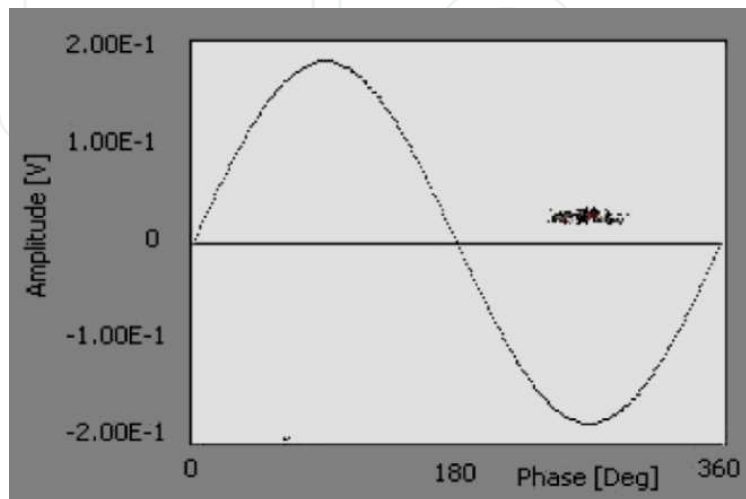

Figure 9. PD Pattern of corona discharges.

In many real cases PD patterns present very different shapes and sometimes with more than only one defect at the same time. For this reason pattern recognition techniques for the discrimination and classification of discharges represent a fundamental instrument for the reliability's evaluation of high voltage electrical apparatus. Many different methods have been proposed in literature to automate the identification of defects through PD pattern recognition. They differ either in presentation of PD data (PD pulse shape data, statistical parameters of these data and pulse density distribution) or in the classification methods (statistical algo‐rithms or neural network (NN)) [20-22]. Recently the use of wavelet analysis and advanced models has provided interesting results in PD denoising processes, pattern recognition and classification of multi-source PD patterns [23,26].

One limit of the classic PD measurement s is due to the wired circuit, signals are dumped or affected by the particular circuit path encountered. In order to overcome these limits wireless measurement have been proposed.

3. Method of moments

The Method of Moments (MoM) in two dimensions has been successfully applied to describe the behaviour of three-dimensional objects that have a highly shielding external structure, for which the hypothesis of perfect electric conductors can be used [11]. Other applications of MoM involving three-dimensional objects composed of voxels or thin wire elements can be

found in [12]. We note S the surface of a metal object considered a perfect conductor (PEC) and n the normal to surface S. By considering an Electromagnetic (EM) stress, E_i denotes the incident electric field, which can be found in the absence of the object having S surface. The presence of an EM field generates surface current J_S on S. The aim of the EM analysis is to determine the current in S. Since no analytical solution can be found for complex geometries only a numerical one can be obtained approximating the current J_S on S into J_i currents on $S^N = \cup_1^N S_i$, (see Fig. 10). Triangular elementary surfaces are used to describe the whole S^N, by introducing edge limiting each triangular faces. Vertexes are the points shared by different triangles. Each triangle, illuminated by external EM field, has its own current, which can conceptually be studied by examining the average current that passes through the three edges. The aim of the MoM is to evaluate each current J_i passing through an edge.

The current on the whole S can be approximated by:

$$\vec{J}_S = \sum_{i=1}^{N} J_i \vec{f}_i(\vec{r}), \tag{1}$$

where N is the number of internal sides, and $f_i(\vec{r})$ are a suitable functions, called basis functions.
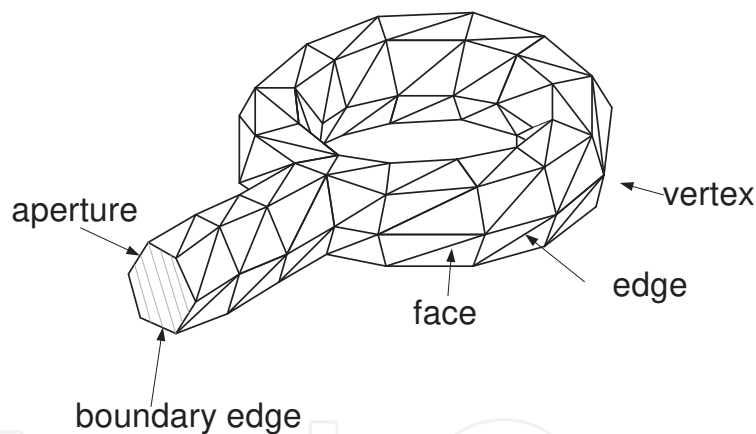

Figure 10. Loop antenna described with triangular surfaces

The basis functions to be used must meet two basic requirements. Indeed, they have to:

- be suitable to be used with an electromagnetic equation.

- Allow modeling with flat triangles. Further useful developments can be found in [27].

Integro-differential equation can be derived by imposing equality between the incident field and scattered field on the boundary condition on S,

$$\hat{n} \times (E_i + E_s) = 0 \tag{2}$$

getting:

$$-E_{inc}^{tan} = -(j\omega \vec{A} - \nabla \varphi)^{tan}, \tag{3}$$

where $\vec{A}$ and φ are the vector and the scalar potential respectively:

$$\vec{A}(\vec{r}) = \frac{\mu}{4\pi} \int_S \vec{J}_S(\vec{r}) \frac{e^{-jkR}}{R} dS' \tag{4}$$

$$\varphi(\vec{r}) = \frac{1}{4\pi\varepsilon} \int_S \sigma(\vec{r}) \frac{e^{-jkR}}{R} dS', \tag{5}$$

with $k = \omega\sqrt{\varepsilon\mu}$.

Such potentials are depending on the local surface current J_S and on the local charge density σ, which can be related to J_S by taking into account the following:

$$\nabla \bullet J_S = -j\omega\sigma \tag{6}$$

The set of equations described here takes the name of Electric Field Integral Equation (EFIE).

Equations 4 and 5 have no analytical solution for a complex S, so an approximation similar to the one used in equation 1 is required, considering only the unknowns J_i set in equation 1.

By considering an edge i shared by two triangles called T_i^+ and T_i^-, it is possible to describe the current in each point M of the triangles, by using the basis functions(see Fig. 11a).

Points (M) belonging to T_i^+ can be detected by means of the distance $\vec{r}$ from an absolute center **O** or through ϱ_i^+distance from the free vertex of T_i^+. Similar remarks can be applied for T_i^-. The choice of the+and-polarities is due to the implementation of a surface current density J_i, which crosses the i side, leaving T_i^+ for T_i^-. In Fig.11 the behaviour of the current in M is associated to the centroids C$^+$ and C$^-$.
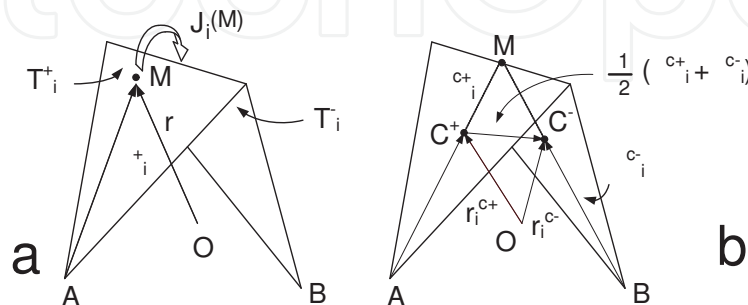

Figure 11. Triangles sharing an internal edge. Focus on the current through the edge (a), focus on centroids.

The purpose of the basis function is to simplify the use of equations 4 and 5, projected in the numerical approximation. The integrals on S are solved for each triangle by taking into account three currents leaving the three edges. The basis function vector is defined by:

$$\vec{f}_i(\vec{r}) = \begin{cases} \dfrac{l_i}{2A_i^+}\vec{\rho}_i & rin\,T_i^+ \\ \dfrac{l_i}{2A_i^-}\vec{\rho}_i & rin\,T_i^- \\ 0 & elsewhere \end{cases} \tag{7}$$

Where l_i is the length of the edge taken into consideration, A_i^+ and A_i^- are the areas of the triangles. Also the following two features are required:

$$\nabla \bullet \vec{f}_i(\vec{r}) = \begin{cases} \dfrac{l_i}{A_i^+} & rin\,T_i^+ \\ -\dfrac{l_i}{A_i^-} & rin\,T_i^- \\ 0 & elsewhere \end{cases} \tag{8}$$

$\vec{f}_i(\vec{r}) = \vec{0}$ on the boundary of S.

It is not possible to solve equation 3 on the whole S, but it can be solved on $S^N = \cup_1^N S_i$, by employing the numerical projection on a N-dimension system. Similarly to the Fourier's sampling a particular function has to be used to project in the N-dimension space, instead of the delta of dirac function here are used the basis functions:

$$\langle \vec{X}, \vec{f} \rangle = \int_S \vec{X} \bullet \vec{f}\, dS, \tag{9}$$

which in the *N-space* becomes:

$$\langle \vec{X}, \vec{f} \rangle \cong \sum_{i=1}^{N} \vec{X}_i \bullet \vec{f}_i A_i, \tag{10}$$

with $\vec{X}$ a vector function. In such a way equation 3 becomes:

$$\langle E_{inc}^{tan}, \vec{f} \rangle = \langle j\omega \vec{A}, \vec{f} \rangle^{tan} + \langle \nabla \varphi, \vec{f} \rangle^{tan}. \tag{11}$$

In equation 11 the gradient is applied on the scalar potential, but considering the following identity (similar to the well known Stokes theorem), it is possible to apply it on the basis function:

$$\langle \nabla \varphi, \vec{f} \rangle = \int_S \nabla \varphi \bullet \vec{f}\, dS = \int_S \nabla \bullet (\varphi \vec{f})\, dS - \int_S \varphi \nabla \bullet \vec{f}\, dS = \int_{\partial S} \varphi \vec{f}\, dS - \int_S \varphi \nabla \bullet \vec{f}\, dS = -\langle \varphi, \nabla \bullet \vec{f} \rangle, \tag{12}$$

with $\vec{f}$ equals to zero on the boundary of both S and ∂S. Finally, by considering a triangle p it is possible to write equation 11 as follows:

$$\left\langle E_{inc}^{p,tan}, \vec{f}_p \right\rangle = \left\langle j\omega \frac{\mu}{4\pi} \int_S \vec{J}_S(\vec{r}) \frac{e^{-jkR}}{R} dS', \vec{f}_p \right\rangle^{tan} - \left\langle \frac{1}{4\pi\varepsilon} \int_S \sigma(\vec{r}) \frac{e^{-jkR}}{R} dS', \nabla \bullet \vec{f}_p \right\rangle^{tan}. \tag{13}$$

To study the effects of the triangle p on the current due to the current of a triangle q(seeFig. 12.a), all the edge currents have to be considered. In Fig.12.b, the interaction between currents on edge of length l_m of p and edge of length l_i of q,is shown.
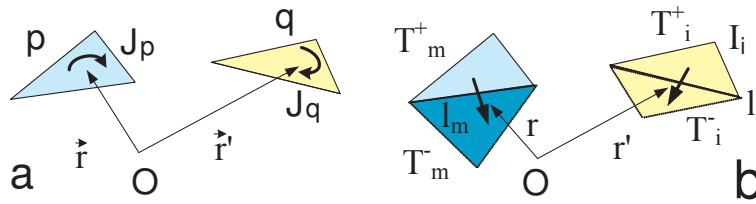

Figure 12. Interactions between currents of different triangles

In equation 13 the inner product has to be considered twice: the formal inner product with $\vec{f}_p$ and the one inside surface integral $\int_S dS'$. By considering initially the first inner product, for edge m, shared by T_m^+ and T_m^-, and also considering value on the centroid as a constant value for all triangle, we can write:

$$\left\langle E_{inc}^m, \vec{f}_m \right\rangle = \int_{T_m^+ + T_m^-} E_{inc}^m \vec{f}_m dS' = E_{inc}^{m,c+} \int_{T_m^+} \vec{f}_m dS' + E_{inc}^{m,c-} \int_{T_m^-} \vec{f}_m dS' =$$
$$E_{inc}^{m,c+} \left(\frac{l_m}{2A_m^+} \rho_m^{c+} \right) A_m^+ + E_{inc}^{m,c-} \left(\frac{l_m}{2A_m^-} \rho_m^{c-} \right) A_m^- = \frac{1}{2} E_{inc}^{m,c+} l_m \rho_m^{c+} + \frac{1}{2} E_{inc}^{m,c-} l_m \rho_m^{c-}, \tag{14}$$

$$\left\langle j\omega \vec{A}(\vec{r}_m^{c+}), \vec{f}_m \right\rangle^{tan} + \left\langle j\omega \vec{A}(\vec{r}_m^{c-}), \vec{f}_m \right\rangle^{tan} = \int_{T_m^+} j\omega \vec{A}(\vec{r}_m^{c+}) \vec{f}_m dS' + \int_{T_m^-} j\omega \vec{A}(\vec{r}_m^{c-}) \vec{f}_m dS' =$$
$$\frac{1}{2} j\omega \vec{A}(\vec{r}_m^{c+}) l_m \rho_m^{c+} + \frac{1}{2} j\omega \vec{A}(\vec{r}_m^{c-}) l_m \rho_m^{c-} \tag{15}$$

$$\left\langle \varphi(\vec{r}_m^{c+}), \nabla \bullet \vec{f}_m \right\rangle^{tan} + \left\langle \varphi(\vec{r}_m^{c-}), \nabla \bullet \vec{f}_m \right\rangle^{tan} =$$
$$\int_{T_m^+} \varphi(\vec{r}_m^{c+}), \nabla \bullet \vec{f}_m dS' + \int_{T_m^-} \varphi(\vec{r}_m^{c-}), \nabla \bullet \vec{f}_m dS' = \varphi(\vec{r}_m^{c+}) l_m - \varphi(\vec{r}_m^{c-}) l_m. \tag{16}$$

The second inner product is inside the vector and scalar potentials, that are due to the current on the edge i:

$$\vec{A}(\vec{r}_m^{c\pm}) = \frac{\mu}{4\pi} \int_{T_i^\pm} J_i \vec{f}_i \frac{e^{-jkR_m^\pm}}{R_m^\pm} dS' = \frac{\mu}{8\pi} J_i l_i \rho_i^{c\pm} \frac{e^{-jkR_m^\pm}}{R_m^\pm}, \tag{17}$$

where $R_m^\pm$ is the distance of the centroids of triangles T_m^+ and T_m^- from the ones of T_i^+ and T_i^-.

In similar way:

$$\varphi\left(\vec{r}_m^{c\pm}\right) = -\frac{1}{j\omega 4\pi}\int_{T_i^\pm}J_i\nabla\bullet\vec{f}_i\frac{e^{-jkR_m^\pm}}{R_m^\pm}dS' = \mp\frac{1}{j\omega 4\pi}J_i l_i\frac{e^{-jkR_m^\pm}}{R_m^\pm}. \tag{18}$$

The double inner product gives a symmetry to the system, the actions of the current i on m and of m on i are similar. The total effect on m is due to an extended summation of index i. In such a way the following equation system holds:

$$ZJ = V, \tag{19}$$

with $Z = [Z_{m,i}]$,

$$Z_{m,i} = \frac{1}{2}j\omega\frac{\mu}{8\pi}\frac{e^{-jkR_m^+}}{R_m^+}l_i\rho_i^{c+}l_m\rho_m^{c+} + \frac{1}{2}j\omega\frac{\mu}{8\pi}\frac{e^{-jkR_m^-}}{R_m^-}l_i\rho_i^{c-}l_m\rho_m^{c-} + \frac{1}{j\omega 4\pi}\frac{e^{-jkR_m^+}}{R_m^+}l_m l_i - \frac{1}{j\omega 4\pi}\frac{e^{-jkR_m^-}}{R_m^-}l_m l_i, \tag{20}$$

$$J = \begin{bmatrix} J_1 \\ \vdots \\ J_N \end{bmatrix}, \tag{21}$$

$$V = \begin{bmatrix} \frac{1}{2}E_{inc}^{1,\,c+}l_1\rho_1^{c+} + \frac{1}{2}E_{inc}^{1,\,c-}l_1\rho_1^{c-} \\ \vdots \\ \frac{1}{2}E_{inc}^{N,\,c+}l_N\rho_N^{c+} + \frac{1}{2}E_{inc}^{N,\,c-}l_N\rho_N^{c-} \end{bmatrix} \tag{22}$$

The vector V contains in each row the effect of the incident electric field due to an external source; if the source is an internal voltage generator, all rows are zero except the one in which is enforced the electric field due to the generator, approximated by the imposed voltage divided by the distance between centroids.

Once defined equation 19, the unknown currents J can be evaluated on the whole surface of the object (see Fig.13.a). Each current starts and ends on a centroid. A dipole moment is definable for each current J_i crossing an internal edge of length l_i (see Fig.11.a):

$$\vec{m}_i = \int_{T_i^+ + T_i^-}J_i\vec{f}_i dS' = \frac{1}{2}l_i J_i\left(\vec{\rho}_i^+ + \vec{\rho}_i^-\right) = l_i J_i\left(\vec{r}_i^- - \vec{r}_i^+\right) \tag{23}$$

The radiated magnetic and electric field, due the dipole of current J_i, in a generic point P (Fig. 12.b) located at a distance $\vec{r}$, are given by:
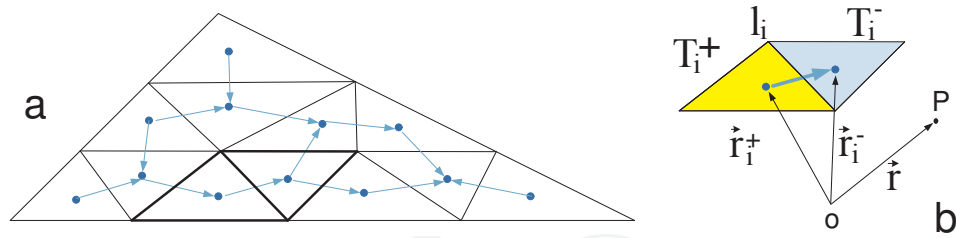
Figure 13. A triangular antenna divided into triangular subparts, in which internal current are shown (a). Particular of the dipole model for the current crossing edge *i* (b).

$$\vec{H}_i(\vec{r}) = \frac{jk}{4\pi}(\vec{m}_i \times \vec{r})\frac{1}{r^2}\left(1 + \frac{1}{jkr}\right)e^{-jkr},$$ (24)

$$\vec{E}_i(\vec{r}) = \frac{\eta}{4\pi}\left(\left(\frac{(\vec{r} \bullet \vec{m}_i)\vec{r}}{r^2} - \vec{m}_i\right)\left(\frac{jk}{r} + \frac{1}{r^2} + \frac{1}{jkr^3}\right) + 2\frac{(\vec{r} \bullet \vec{m}_i)\vec{r}}{r^4}\left(1 + \frac{1}{jkr}\right)\right)e^{-jkr}.$$ (25)

4. Antenna modeling with method of moments

The aim of this study is to create a model to describe the behaviour of PD signal probe. Antennas can be easily designed with commercial software like Matlab® in which suitable tools also create the Delaunay triangulation.

The simplest antenna to be designed is the monopole antenna, shown in Fig.14. In order to create the 20 cm long monopole two rectangles have been created, one thin in which only a line of triangle is needed, another bulky.By considering the possible interactions between the two triangles, problems arise. There is an edge shared between three triangles (red, yellow, blue). The current of this edge will be divided into 2 sub-currents and another row and unknown is set in equation (6).
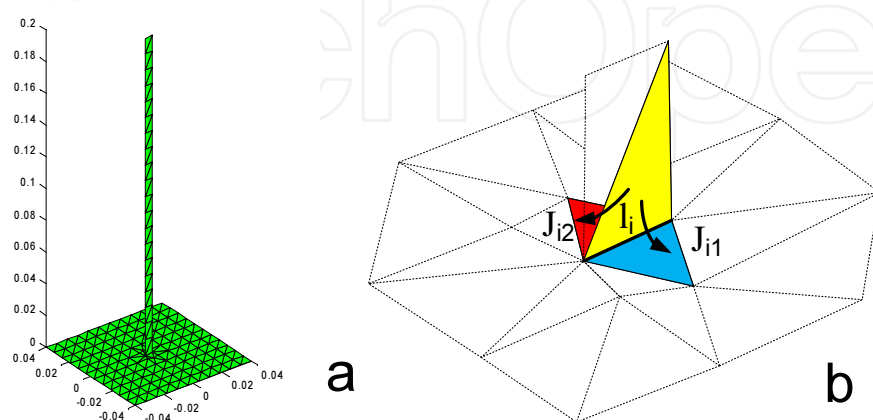

Figure 14. Discrete surface MoM model of the monopole antenna.

Similarly all non-planar antennas are treated. In Fig. 15 the triangular antenna and the spherical one are shown. The triangular antennas simulates a planar 20 cm equilateral triangle. The sphere has 6 cm diameter.
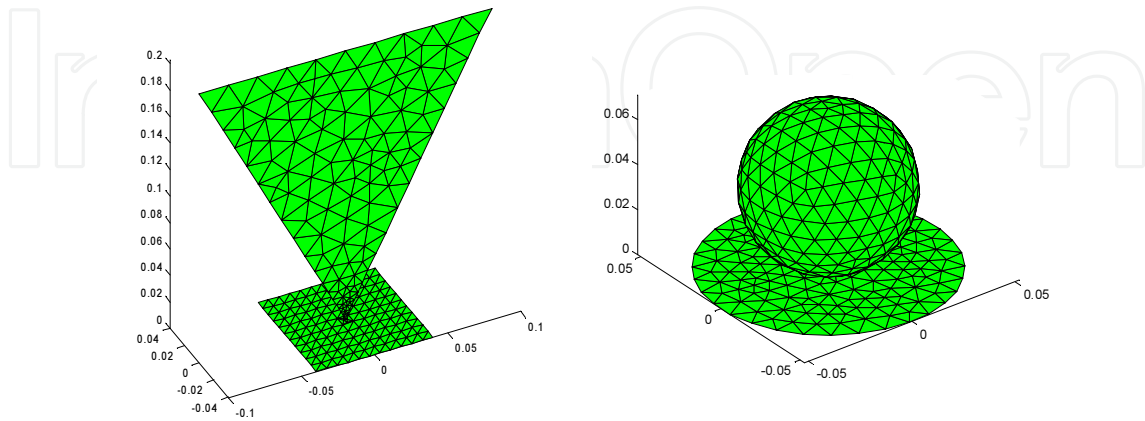

Figure 15. Discrete surface MoM model of the triangular and spherical antennas.

In Fig.16 an electronic power device is sketched: two metal plates, normally at different voltage, during a partial discharge are metallically linked by the discharge path.
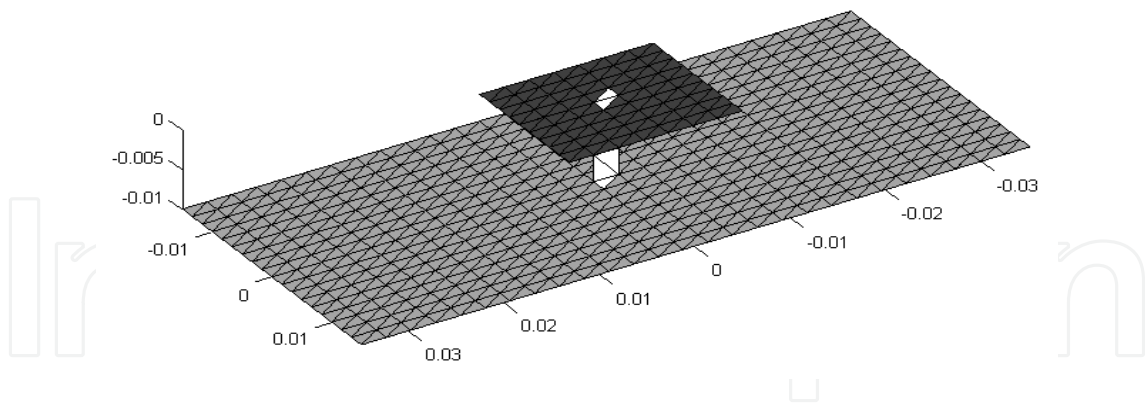

Figure 16. Discrete surface MoM model of the emitting source.

The numerical model allows to feed all the antennas in two different ways. The first one uses a voltage generator, set between the antenna (upper object) and ground plate (bottom metallic plate). The other way takes into account the illuminating external field on the surface of the whole object. In order to simulate the transmission of fault EM signal and its receiving, the power device is fed by generator and the other antennas are used as probes, so the provided voltage on the linking edge is studied.

As previously explained the source of the EM field illuminating the probes is given by the discharge current flowing through the discharge path, which is due to the ionized air gap inside of insulation, and embraces previously damaged materials and metallic surfaces. A full characterization of the exact discharge channel is beyond the scope of this work and also for sake of simplicity the discharge path is simulated with a metallic wire in which the discharge current flows unhindered. Then neglecting particular behaviour to the geometry of the discharge channel, scrupulous attention is paid to the waveform of the current, the harmonic content, which will characterize the fidelity of the receiving probes, is studied.
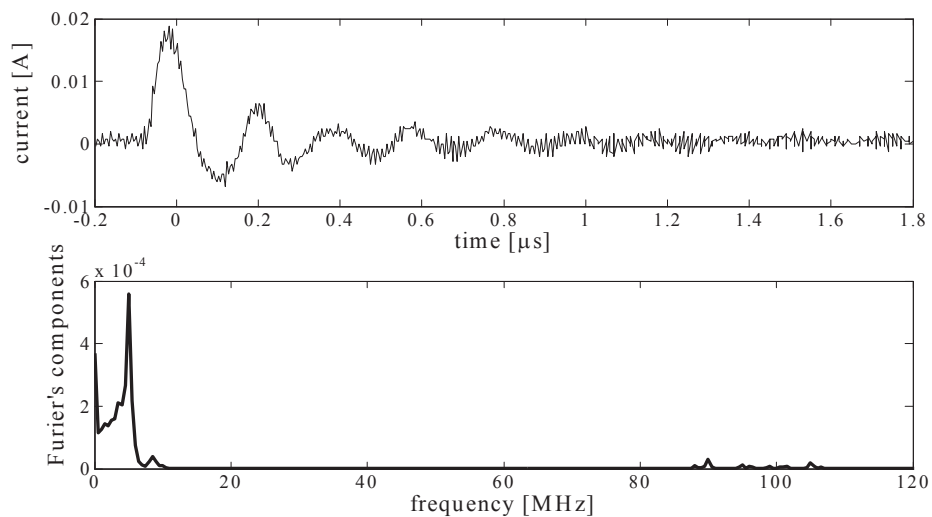

Figure 17. Discharge current and Fourier spectrum. Noise is on 90-110 MHz range.

In Fig.17, a PD signal is represented, which is characterized by an underdamped oscillation. This latter propagates until the energy balance is once again stable, and the charges back to be imprisoned in the dielectric. In order to study the transient PD signal Discrete Fast Fourier Transform (DFFT) has to be used. The PD signals may have a faster or slower evolving, but roughly the spectrum of interest is contained in a [0-200MHz] window. This aspect allows characterizing the type of receiving probes. Unfortunately, in the environment in which PD signals are generated, other signals, that should affect in a limited way the diagnostic tool, are present. PD signal of Fig.17intentionally contains a part of noise that will interact with the probes receivers.

Once defined the behaviour of the PD current, it is possible to characterize the behaviour of the source system, focusing at 20 cm from the discharge, chosen as a compromise between the possibility of bringing a wireless sensor to the faulty part and the need to maintain a safe distance or in other cases distance imposed by the presence of screens, shields and spacers.The PD discharge path has a normal direction with respect to the ground plate and an unitary current source is applied within the range of [0-1000MHz]. The simulated z-component of the

electric field at a distance of 20 cm, is shown in Fig.18. The electric field profile is growing with the frequency, similar to the one of a dipole with its dimension equal to the discharge path.
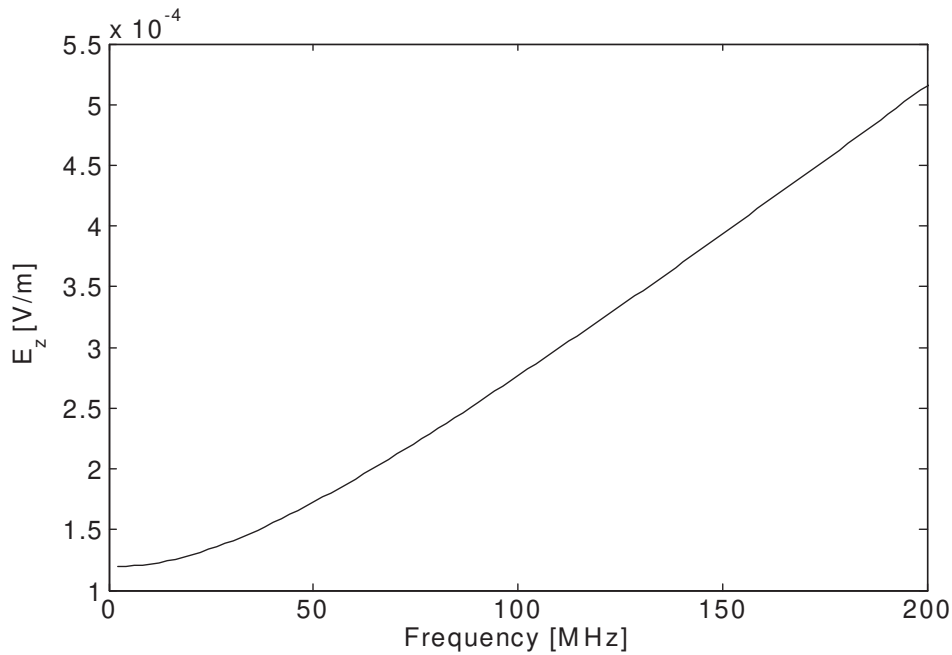

Figure 18. E_z field generated by the discharge at a horizontal distance of 20 cm. Only the 0-200 MHz interval is shown.

In order to compare the different antennas behaviour a particular transfer function is considered:

$$H = \frac{V_{received}}{E_{incident}} \left[m \right] \tag{26}$$

where $V_{received}(\omega)$ is the voltage response of antennas, illuminated by the incident electromagnetic field.

The incident EM field due to the PD current, which is function of the signal frequency content, has to be computed. The received voltages can be computed by simulating the response of the antenna illuminated by the incident EM field. The voltage response is due to both source and antenna impedance behaviour. The three transfer functions corresponding to the three antenna typologies are plotted in Fig. 19considering the above mentioned frequency range.

As it can be seen, the monopole antenna provides the highest gain but its profile is characterized by a resonant peak centered at about 450 MHz. The triangular antenna shows a resonant peak centered in about 400 MHz but with lower amplitude with respect to the former. On the contrary, the spherical antenna shows a flat bandwidth with the lowest amplitude among the three.
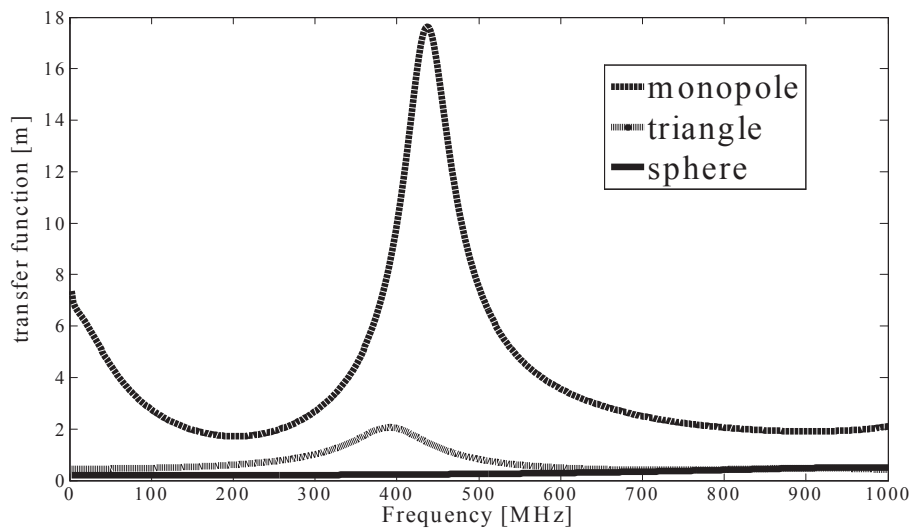
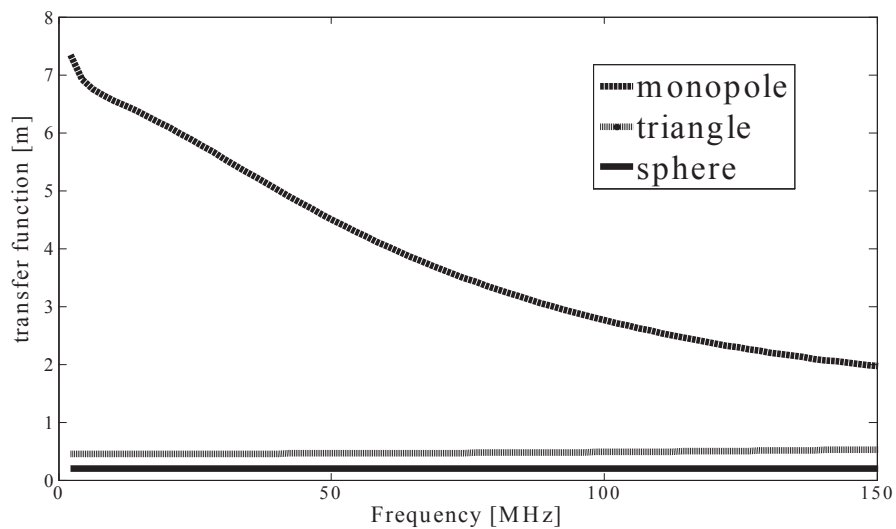**Figure 19.** Transfer function of the three antennas.

Figure 20. Transfer function of the three antennas for the range of 0-150MHz.

In Fig.20, the different transfer functions are plotted in the frequency range going from 0 to 200 MHz. The spherical and triangular antennas show an almost flat behaviour while the monopole is characterized by a significant decrease in amplitude. It is easily to argue that these different profiles have a different impact on the shape of the recorded PD signals. The selection of a specific profile depends on the application, e.g. PD measurements in dc, ac and rectangular (adjustable speed drive applications) voltage supply. A procedure able to evaluate the signal distortion of the different antennas has been developed to select the antenna able to fit the separation and identification requirements.

5. Transmission of Signals

In order to test the different antennas, bursts of damped pulses were simulated with super-imposed high frequency noise in the frequency range of 0-200MHz. The performances of the three antenna configurations were evaluated considering the simulated received signals. An example of the normalized voltage response of the three antennas is plotted in Figure 21. According to Fig. 19, it was found an amplitude reduction of-10 dB and-14 dB for the triangular and spherical antennas with respect to the monopole probe.
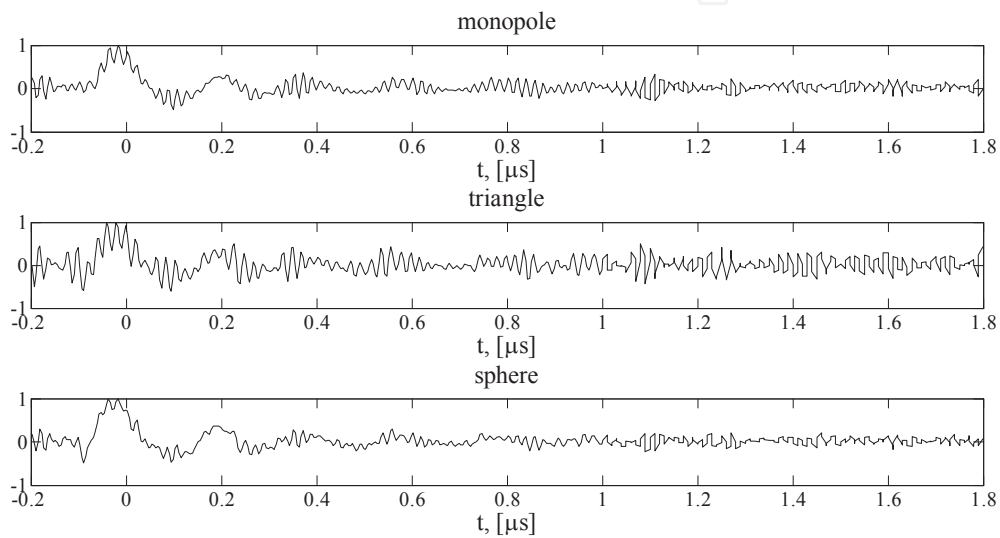

Figure 21. Time profiles of the received voltage.

Moreover, the high frequency noise has the highest influence on the pulse signal received by the triangular antenna since its transfer function reduces the amplitude of the pulse signals and amplifies the superimposed noise. The opposite considering the monopole configuration, while the flat bandwidth of the spherical antenna reduces both the amplitude and the super-imposed noise of the received pulse signal. A dedicated procedure has been developed in order to validate this empirical evaluation.

The proposed validation procedure is based on the classification of the autocorrelation function (ACF) of the PD signals, via the K-Means classification algorithm [10]. The ACF has been proposed for its ability to synthesize both the time and frequency domain features as well as to be less affected by superimposed high-frequency noise, random truncation of the pulse-tail (frequency leakage) and different trigger activation. The ACF is evaluated by taking into account the following expression:

$$R_S = \int_{-\infty}^{\infty} s(t)s(t+\tau)dt \tag{27}$$

where $s(t)$ represents the time behaviour of the simulated PD signal in discrete time domain. In order to compare the shape of signals with different energy, the normalized ACF in discrete time domain has been here adopted:

$$R_S[k] = \frac{\sum_{i=1}^{N} s(i)s(i+k)}{N} \frac{1}{E_S},$$
(28)

Where $s(i)$ is the signal digital sample, N is the number of digital samples, E_S is the energy of the signal:

$$E_S = \frac{\sum_{i}^{N} s(i)^2}{N}$$
(29)

Fig.s22 and 23 show the NACF of the signals reported in Fig. 17 and 21, respectively.

The Pearson correlation index, ϱ, is used to compare the different NACF with the emitted one. The covariance between two NACFs can be evaluated by the following expression:

$$cov(R_{S1}, R_{S2}) = \frac{\sum_{k=1}^{N} \left[R_{S1}(k) - \bar{R}_{S1} \right] \bullet \left[R_{S2}(k) - \bar{R}_{S2} \right]}{N-1},$$
(30)

where $\bar{R}_{S1}$ and $\bar{R}_{S2}$ are the mean value of NACFs.

The Pearson correlation index is:

$$\rho = \frac{cov(R_{S1}, R_{S2})}{\sqrt{var(R_{S1})} \bullet \sqrt{var(R_{S2})}},$$
(31)

where $var(R_{S1})$ and $var(R_{S2})$ are the variance of the NACFs.

The distance in the NACF metric can be assumed as:

$$d_\rho = \sqrt{2(1-\rho)}$$
(32)

Previous investigations established a $d_\varrho < 0.4$ as a good threshold level in the PD shape comparison. The differences between the transmitted and the received signals using the three different configurations, evaluated considering the distance of equation 32, are reported in Table 1.
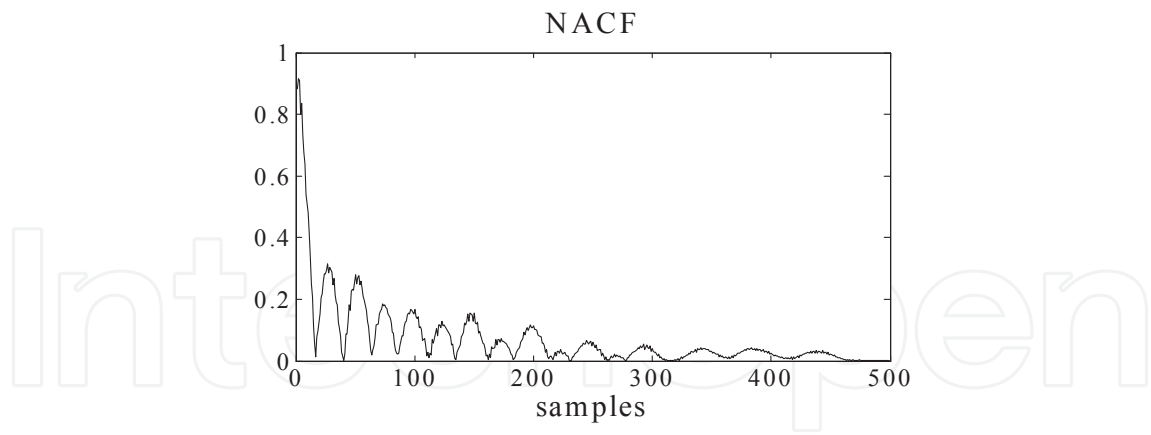
Figure 22. NACF of the PD current of Figure17.
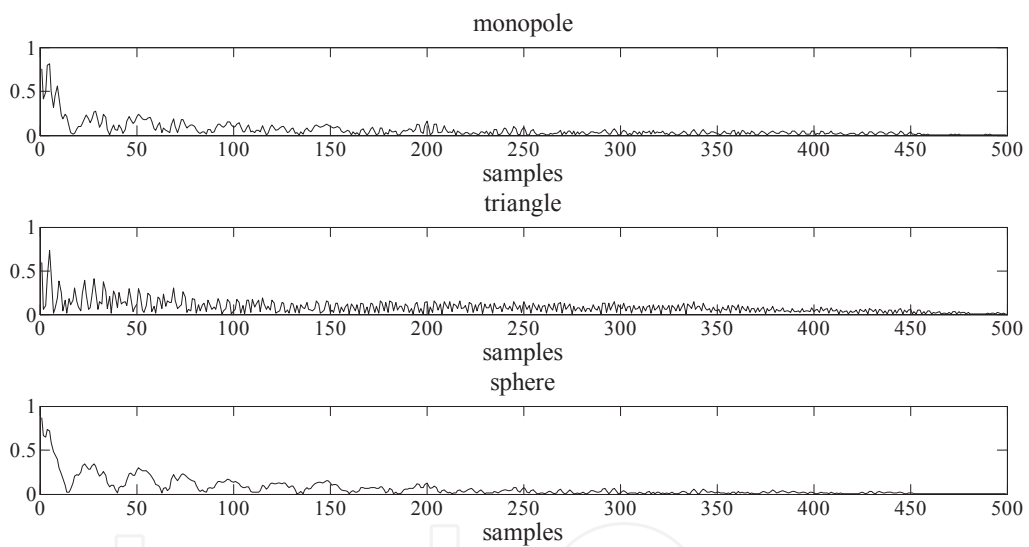
Figure 23. NACFs of the transmitted signals of Figure21.

Distance		
Monopole	**Triangle**	**Sphere**
0.39	0.96	0.29

As it can be seen, the monopole and the spherical antenna preserve the pulse shape in almost similar way while the triangle's received signal is affected by noise and it is groped far from

the PD signal. Due to the different attenuation in the different frequency ranges (Fig. 19), the monopole antenna tends to modify differently the shape of signals generated by the same source. This can induce an over classification in separation procedure that is, the generation of more classes than PD sources. The spherical antenna, due to its flat bandwidth, seems to be the most suitable wireless probe for ac applications.

6. Discussion

The table I shows that the most suitable probes for the identification of partial discharge signals are the monopole probe and the spherical probe. This evaluation was obtained using one of the simplest classification algorithms, certainly other more advanced algorithms may change this rating, and also the use of digital filters in the same implementation may overturn the comparison. The use of filters or the use of more elaborate techniques of signal processing goes beyond the intentions of this chapter. Therefore, the comments will be expressed only in relation to the analogical performance of probes.

6.1. Monopole antenna

The monopole probe has a high gain, superior to the others. This is one of the key aspects in the evaluation of partial discharge phenomena that makes it attractive: the discharges take place within structures often shielded, for which the outgoing signals are weak. The use of too attenuating probe could make the measurement insufficient and the monopole can solve this issue. However, the use of this probe in the industrial environment is not wise since it could involve the absence of higher harmonics. Indeed, their contribution can modify the shape of the signal and even changing the initial instant of the discharge. Such behaviour, in the diagnosis of PD phenomenon, is not acceptable, since the determination of the type of discharge (internal, surface, corona, etc..) is based on the presence of a greater or lesser occurrence of discharges at certain angles of the sine wave function. One way to change the behaviour of the monopole is to change its length, but this length cannot be sufficiently modified to remove the effect of resonance. A simple way to try to mitigate the effect of the resonance is to insert appropriate RLC circuits. UWB antennas are actually filters, which introduce dependences between the transmitter and the receiver frequencies. Therefore such kind of antennas can be treaded. Generally, antennas have linear and passive behaviour, and input impedance can be represented by means of the canonical forms of Foster [28-30].The structure shown in Fig.24 is suitable to represent electric antenna as the electric dipole and monopole.In order to modify the behaviour of the antenna, the electric model of the antenna is required. The numerical implementation of the antenna gives the complex impedance used in the equation 19. The equivalent circuit has to show a similar behaviour for all the harmonic of interest. By following the steps in [28] the value of C_0 is set by taking the value of the capacity presented by the antenna at low frequencies; the value of L_0 is initially set to cancel the imaginary part of impedance at the first resonance frequency. It is required that the first RLC parallel branch has a resonant frequency corresponding to the first maximum of the real part

of impedance. By adding more RLC parallel branch the impedance profile can be easily reproduced. Once the circuital model of the antenna is reproduced, new real RLC parallel branch can be used to modify the behaviour of the antenna by mitigating the resonance effect.
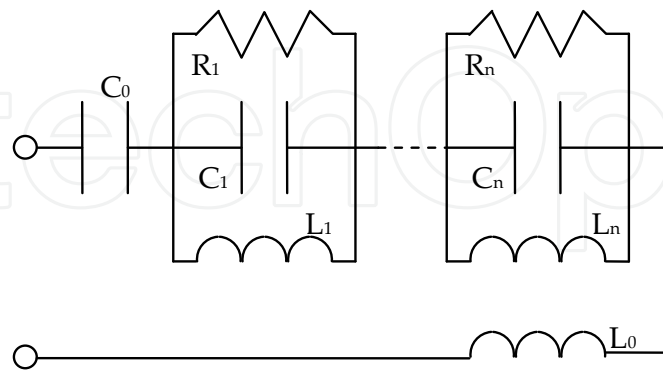

Figure 24. Foster's canonical form for an electrical antenna.

6.2. Triangle antenna

The triangular antenna has a resonance similar to the one of the monopole and shares the same height. The triangular antenna presents an uninteresting behaviour already even used under the best conditions (propagation orthogonal to the surface, absence of high frequencies). Therefore, it is not useful to make changes to improve performances.

6.3. Spherical antenna

The spherical antenna is the true omnidirectional antenna and its performance does not vary by changing its inclination. Then, it presents suitable features to build the PD probes. However, it has a small gain, but this issue can be overcome by using appropriate amplifiers.

7. Conclusion

In this chapter the design of PD receiving antennas has been shown. Three different antennas were simulated by means of the method of moments. Received PD signals have been analyzed by the employment of the classification algorithm, based on the autocorrelation function (ACF) of the signals. The difference in the classification of the received signals has been explained by studying the aspects of the transmitted signals due to the shape of the receiving antennas. The best performances were obtained with the spherical antenna. Indeed, it exhibits an omnidirectional pattern and reliability for reproducing the shape of the partial discharge signal. Thus, this kind of antennas can be suitable to acquire PD pattern to determine the particular type of PD activity.

Author details

Fabio Viola[*] and Pietro Romano

*Address all correspondence to: fabio.viola@unipa.it

Department of Energy, Information engineering, Mathematical models – DEIM, University of Palermo, Palermo, Italy

References

[1] Yin, X.-C., Ruan, C.-L., Mo, S.-G., Ding, C.-Y., and Chu, J.-H. A compact ultra-wide band microstrip antenna with multiple notches. Progress In Electromagnetics Research, PIER 84, 2008, 321–332.

[2] Lamultree S., and Phongcharoenpanich, C. Bidirectional ultra-wide band antenna using rectangular ring fed by stepped monopole. Progress In Electromagnetics Research, PIER 85, 2008, 227–242.

[3] Akhoondzadeh-Asl, L., Fardis, M., Abolghasemi, A., and Dadashzadeh, G. Frequency and time domain characteristic of a novel notch frequency UWB antenna. Progress In Electromagnetics Research, 2008, PIER 80, 337–348.

[4] Notice of Proposed Rule Making, Revision of Part 15 of the Commission's Rules Regarding Ultra-Wideband Transmission Systems. Federal Communications Commission (FCC), ET Docket 98-153, 2002.

[5] B. A. Fruth and D. W. Gross, Phase Resolving Partial Discharge Pattern Acquisition and Frequency Spectrum Analysis. IEEE 4th Intern. Conf. Propertie, Application of Dielectr. Materials (ICPADM), Brisbane, Australia, paper 6207, 1994.

[6] Baker, P.C. and Judd, M.D. and McArthur, S.D.J.A frequency-based RF partial discharge detector for low-power wireless sensing. IEEE Transactions on Dielectrics and Electrical Insulation2010; 17(1) 133-140.

[7] P. J. Moore, I. E. Portugues, and I. A. Glover, Partial Discharge Investigation of a Power Transformer Using Wireless Wideband Radio-Frequency Measurements.IEEE Trans. On Power Delivery2006; 21(1), 528-530.

[8] A. Cavallini, A. Contin, G. C. Montanari and F. Puletti, Advanced PD Inference in On-Field Measurements. Part.1: Noise Rejection. IEEE Trans. on Dielectrics and Electrical Insulation 2003;10(2) 216-224.

[9] A. Cavallini, M. Conti, A. Contin, G. C. Montanari Advanced PD inference in on-field measurements. Part 2: Identification of defects in solid insulation. IEEE Trans. on Dielectrics and Electrical Insulation 2003; 10(3) 528-538.

[10] A. Contin, S. Pastore, Classification and separation of partial disharge signals by means of their auto-correlation function evaluation. IEEE Trans. On Dielectrics and Electrical Insulation2009; 16(6)1609-1622.

[11] S. M. Rao, D. R. Wilton AND A. W. Glisson, Electromagnetic Scattering by Surfaces of Arbitrary Shape. IEEE Trans. On Antennas snd Propagation 1982; 30(3), 626-629.

[12] Wang, J. H., Generalized moment methods in electromagnetics, Wiley Interscience Publication, 1991.

[13] Makarov, S. N., Antenna and EM Modelling with Matlab, Wiley Interscience Publication, 2002.

[14] G. Ala, R. Candela, F. Viola, Detection of Radiated EM Transients by Exploiting Compact Spherical Antenna Features, Recent Patents on Electrical Engineering 2011, 4, 202-208.

[15] J.C. Anderson. Dielectrics; Chapman & Hall, London 1964.

[16] L. Simoni. Proprietà dielettriche e scarica dei materiali isolanti elettrici; Clueb, Bologna, 1996.

[17] L.A. Dissado, J.C. Fothergill. Electrical Degradation and Breakdown in Polymers, Peregrinus, 1992.

[18] A. Pedersen. Partial Discharges in Voids in Solid Dielectrics. An Alternative Approach. 1987 Annual Report Conference on Electrical Insulation and Dielectric Phenomena, IEEE publication 87 CH2462-0, 1987, 58-64.

[19] IEC Standard 60270. High-Voltage Test Techniques-Partial Discharge Measurements; 2000.

[20] A. Krivda. Recognition of Discharges. Discrimination and classification. Delft University Press, Delft, 1995.

[21] E. Gulski. Computer-aided Recognition of Partial Discharges Using Statistical Tools; Delft University Press, Delft, 1991.

[22] R. Candela, G. Mirelli, R. Schifani PD Recognition by Means of, Statistical and Fractal Parameters and Neural Network. IEEE Transactions on Dielectric and Electrical Insulation 2000; 7(1), 87-94.

[23] X Ma, C. Zhou,I.J. Kemp Interpretation of wavelet analysis and its application in partial discharge detection. IEEE Trans. on Dielectric and Electrical Insulation 2002; 9(3) 446-457.

[24] R. Candela, P. Romano. An improved MSD-based method for PD pattern recognition. 2007 Annual Report Conference on Electrical Insulation and Dielectric Phenomena, October Vancouver BC, Canada October 14-17, 2007, 204-207.

[25] Ala G, Candela R, Romano P, Viola F. Simplified Hybrid PD Model in Voids. 8th IEEE Symposium on Diagnostics for Electrical Machines, Power Electronics &

Drives. Bologna, 5-8 September 2011, 451-455, IEEE, ISBN: 978-1-4244-9303-6, doi: 10.1109/DEMPED.2011.6063662.

[26] Di Silvestre L., Romano P., Viola F. Simplified Hybrid PD model in Voids: Pattern Validation, 4th International Conference on Power Engineering, Energy and Electrical Drives –Powereng, 13-17 may 2013, Istanbul,Turkey.

[27] A. W. Glisson, On the development of numerical techniques for treating arbitrarily-shaped surfaces. Ph.D. dissertation, Univ. Mississippi, 1978.

[28] Foster, R. M. A reactance theorem. Bell Systems Technical Journal, 1924;3(2) 259–267.

[29] S. B. T. Wang, A. M. Niknejad, R. W. Brodersen, Circuit modeling methodology for UWB omnidiretional small antennas. IEEE Journal on Selected Areas in Communications2006; 24(4)871-877.

[30] M. Hamid, R. Hamid, Equivalent Circuit of Dipole Antenna of Arbitrary Length. IEEE transactions on Antennas and Propagation 1997; 45(11) 1695-1696.